SYNTHESIS OF LAYERED TITANOSILICATE JDF-L1 FOR FABRICATION OF COMPOSITE POLYAMIDE 6 FILM

Cesar Rubio[a], *Elena Piera*[b], *Miguel Ángel Caballero*[b], *Carlos Téllez*[a*], *Joaquín Coronas*[a]

[a] Chemical and Environmental Engineering Department and Nanoscience Institute of Aragón. Universidad de Zaragoza, 50018 Zaragoza, Spain

[b] Research and Development Department. Nurel S.A., Ctra. Barcelona km 329. 50016 Zaragoza, Spain

*Corresponding author: Dr. Carlos Téllez. Universidad de Zaragoza. c/ Mariano Esquillor s/n. 50018 Zaragoza. Spain. Phone: 34 976 762897. Fax: 34 976 761879. e-mail: ctellez@unizar.es

ABSTRACT

In clay polymer nanocomposite technology, nowadays there is concern about the safety and environmental effects of the nanometric materials. In this work, sheets of layered titanosilicate JDF-L1 were synthesized with a size of 5.3 μm and thickness of 115 nm and used to fabricate composite polyamide 6 (PA6) films. The JDF-L1 synthesis was scaled in one pot and the rosette-like particles obtained were disaggregated using a simple process with NaOH solution. The composite with 2 wt% of disaggregated JDF-L1, characterized by X-ray diffraction and electron microscopy, showed parallel orientation (with respect to the film itself) and good dispersion of the sheets. The composite had a similar barrier effect as the PA6 and its mechanical properties did not deteriorate. This opens up the use of this composite as a packing material providing other properties, such as a biocidal effect and synergy effect in combination with other additives.

KEYWORDS. Layered Titanosilicate, Polyamide, Hybrid composites, Permeation, Directional orientation

1. Introduction

Layered silicates and zeolites, and their respective exfoliated materials, are useful for catalysis (Corma et al., 1999; Wu et al., 2004; Centi and Perathoner, 2008; Roth et al., 2014), enhancing the permselectivity of zeolite-polymer nanocomposite membranes (Jeong et al., 2004; Choi et al., 2008; Rubio et al., 2015), the immobilization of enzymes (Corma et al., 2001) and producing layered silicate-polymer nanocomposites with improved tensile properties (Wang and Pinnavaia, 1998). This is due to their fine particles, with high aspect ratios and a theoretical thickness as low as that of a single layer in the case of exfoliated materials. JDF-L1 is a layered titanosilicate, also reported as AM-1 (Anderson et al., 1995; Lin et al., 1997) and NTS titanosilicate (Veltri et al., 2006), whose structure was established by Roberts et al. (Roberts et al., 1996) in 1996 and later refined by Ferdov et al. (Ferdov et al., 2002). It is a member of the microporous OPT (octahedral–pentahedral–tetrahedral) family of framework silicates (Rocha and Lin, 2005). The formula of JDF-L1 is $Na_4Ti_2Si_8O_{22}\cdot 4H_2O$ and it contains five-coordinated Ti (IV) ions in the form of TiO_5 square pyramids where each of the vertices of the base is linked to SiO_4 tetrahedra $[TiO\cdot O_4(SiO_3)_4]$ forming continuous sheets with exchangeable interlamellar Na^+ ions (Anderson et al., 1995; Roberts et al., 1996; Lin et al., 1997; Veltri et al., 2006). In Fig. 1 it can be observed that JDF-L1 layers have five-membered rings running parallel to each other ([100] or [010] equivalent directions) consisting of four SiO_4 tetrahedra and one TiO_5 pyramid. In the [001] direction, the layers also contain six-membered rings composed of two square pyramids and two pairs of tetrahedra giving rise to a pore size across the layers of approximately 3 Å (smaller than the kinetic diameter of O_2: 3.46 Å) (Galve et al., 2011). Using seeded hydrothermal synthesis (Rubio et al., 2009), relatively small (3 x 3 μm) JDF-

53 L1 crystals can be achieved while the synthesis time needed to reach a high crystalline
54 product is reduced. Galve et al. (Galve et al., 2013) made Mixed Matrix Membranes with a
55 combination of JDF-L1 and MCM-41 fillers. These gave rise to a synergy effect with a
56 better dispersion of the filler compared with using MCM-41 only.

57 In recent years, there has been an increasing interest in the so-called
58 nanocomposites incorporating nanostructured elements due to the changes that provide in
59 the composition and structure compared to conventional composites. The layered silicates
60 dispersed as a reinforcing phase in the polymer matrix is one of the most important ways to
61 prepare hybrid organic-inorganic nanocomposites (Giannelis, 1996). The use of organoclay
62 polymer nanocomposites as precursors has spread to various polymer systems, but for
63 making nanocomposites the exfoliated monolayers of clay must be uniformly dispersed in
64 the polymer matrix. Polymer-clay compounds containing conventional aggregates of sheets
65 show improved rigidity while decreasing the impact strength and elongation, while all the
66 physical properties of nanocomposites made with exfoliated clay are improved, as seen in
67 the case of the nanocomposite of clay-Nylon 6 (LeBaron et al., 1999; Daud et al., 2009;
68 Zhang and Yang, 2012). In particular, polyamide-based composites with inorganic fillers
69 have been the focus of important research since the pioneering work done by Toyota on the
70 synthesis of Nylon-6 composites with improved mechanical and thermal properties as
71 compared to the pure polymer (Kojima et al., 1993; Usuki et al., 1993). Polyamide-based
72 composites have been applied for mechanical reinforcement in automotive and aerospace
73 applications and also for flame retardancy (Cai et al., 2010). Additionally, the possibility
74 has been explored of reusing (by layered silicate reinforcement) spent polyamide
75 nanocomposites (Aldousiri et al., 2012). The sheets also provide other benefits as the

76 impermeability of the sheets to some gases creates tortuous paths to permeate through the
77 nanocomposite. The gas permeability through the nanocomposite can be reduced between
78 50 and 500 times with a small charge (Choudalakis and Gotsis, 2009). Finally, silylation of
79 JDF-L1 have been done to prepare titanosilicate-PVC nanocomposites (Park and Jung,
80 2011).

81 Exfoliated materials and nanomaterials are important in the fabrication of
82 nanocomposites to improve the barrier effect of the target polymer (Alix et al., 2012;
83 Mihindukulasuriya and Lim, 2014). An example is their use for food packaging in which
84 nanotechnology plays a key role in antimicrobial functions, oxygen scavenging and shelf-
85 life extension of the food (Vähä-Nissi et al., 2014). However, with the increasing
86 commercialization of nanomaterials, governments are becoming more concerned about the
87 safety and environmental effects of the use of products containing these materials. For
88 instance, in 2009 the European Food Safety Association (EFSA) was requested by the
89 European Commission to provide a scientific opinion on potential risks arising from
90 nanoscience and nanotechnologies on food and feed safety. Echegoyen et al. (Echegoyen
91 and Nerín, 2013) demonstrated the migration of silver nanoparticles and other
92 nanomaterials from three commercially available food containers. The plastic nanoparticles
93 found suggest that these nanoparticles are used for a better dispersion and stability of the
94 silver nanoparticles during the manufacture of the plastic container. Due to the risk
95 associated with nano-sized components, JDF-L1 has not been exfoliated but simply
96 disaggregated to handle micron-sized sheets with thicknesses slightly above 100 nm.
97 Furthermore, JDF-L1 can be modified by ion exchange with Ag^{+}, Zn^{2+} and Cu^{2+} to enhance
98 its biocide activity (Pérez-Carvajal et al., 2012) and no dispersant is necessary for proper

distribution in the composite, thus avoiding nanoparticles. In this work JDF-L1 was synthesized and disaggregated with a simple process where only NaOH is used. This process was scaled-up. Finally, disaggregated JDF-L1 was combined with polyamide 6, achieving a good orientation and homogeneous dispersion of the filler.

2. Experimental details

2.1. Preparation of materials

The synthesis of JDF-L1 is based on a seeded hydrothermal synthesis (Rubio et al., 2009). For the synthesis in a 40 mL autoclave, 26.2 g of gel with a molar composition of 4.2 SiO_2:1 TiO_2:2.9 Na_2O:101 H_2O was made. In addition, 10.0 g of sodium silicate solution (27 wt% SiO_2, 8 wt% Na_2O, Merck) was mixed with 6.5 g of deionized water and 1.4 g of NaOH (99.0 wt%, Scharlab); then 8.2 g of $TiCl_3$ solution (20 wt% in 3 wt% HCl, Alfa Aesar) and 79 mg of seeds (grounded JDF-L1) were added. After stirring for 1 h at room temperature, the resulting gel was degassed for 5 minutes in an ultrasonic bath and transferred into a 40 mL Teflon-lined autoclave. The crystallization was carried out at 230ºC for 24 h. After filtering and washing with deionized water and drying at 100ºC overnight, 4.2 g of powder was obtained. In the same way, the synthesis was carried out in a 150 mL and a 400 mL Teflon-lined autoclave (Berghof DAB-3 400 mL) where the amount of gel was multiplied by 3 and 10, and that of seeds by 3 and 20, respectively.

To disaggregate the JDF-L1, a similar procedure to that of Galve et al. (Galve et al., 2011) was used. The solution was a mixture of aqueous solutions of a salt containing the cation (hexadecyltrimethylammonium) and tetrapropylammonium hydroxide solution (TPAOH) which provides high pH. The reaction lasted for 16 h in a temperature range of 80 to 95ºC. This process did not swell the JDF-L1, for which a more elaborated process is

122 needed (Rubio et al., 2010). For this reaction, 2.9 g of hexadecyltrimethylammonium
123 bromide (CTAB, 98.0 wt%, Sigma-Aldrich) was added to 6.1 mL of HPLC grade water
124 (Fisher Scientific). Subsequently 5.9 mL of TPAOH solution (1.0 M in H_2O, Sigma-
125 Aldrich) and 0.5 g of synthesized JDF-L1 were added. The resulting mixture was
126 transferred to a round-bottomed flask and the reaction was carried out under reflux and
127 vigorous stirring for 16 h at 80ºC. After this time, the solution was centrifuged at 10000
128 rpm for 10 min, removing the supernatant and adding deionized water. The centrifugation-
129 washing process was repeated twice more and the material obtained was dried at 100ºC for
130 12 h. It was observed by SEM that not all the material was disaggregated, so other methods
131 were tested. The same solution was prepared without CTAB and in another assay the
132 TPAOH was replaced by 0.24 g of NaOH. Both methods were effective. Finally, a NaOH
133 solution was tested, this method being most effective. Once it was known that the method
134 was appropriate it was repeated with a higher amount of JDF-L1 (~ 35 g). 35 g of JDF-L1
135 were added to a solution of 16.5 g of NaOH in 420 mL of HPLC grade water (0.92 M). The
136 reaction was carried out in a round-bottom flask of 500 mL under reflux and vigorous
137 stirring for 16 h at 80ºC. Subsequently, due to the large volume of the dispersion, it was
138 filtered with a Büchner and Kitasato using two filter papers (2-4 μm pore) and the solid was
139 washed with 800 mL of deionized water. The material obtained was dried at 100ºC for 12
140 h.

141 The purpose of the disaggregated JDF-L1 was its use as an additive in polymeric
142 films of polyamide 6 (PA6) to increase the oxygen barrier effect due to its characteristics.
143 This type of film is fabricated by the company Nurel SA. The films were produced by
144 extrusion from pellets made by Nurel SA of PA6 and PA6 with a load of 2 wt% of

disaggregated JDF-L1. Pellets of PA6 and JDF-L1@PA6 were prepared in a lab-scale polymerization reactor with a capacity of 1.5 L. Before the polymerization stage, a dispersion process (2 h, 900 rpm, 90ºC) was used in order to disperse the JDF-L1 into the monomer (caprolactam). The hydrolytic polymerization of caprolactam in the autoclave was carried out with a stirring device at pressures up to 5 bar and an elevated temperature (260ºC) in the presence of water and a weak acid. In a second stage, further polymerization and the removal of volatile components such as water was carried out until the desired viscosity was reached.

2.2. Characterization

X-ray diffraction (XRD) (using a Rigaku/Max System diffractometer, CuKα radiation with λ=1.5418 Å and a graphite monochromator) was carried out on most of the samples. The X-ray fluorescence (XRF) analyses were carried out with a THERMO ELECTRON ARL model ADVANT'XP with a rhodium tube. Thermogravimetric analyses (TGA) were performed in a TGA/DSC 1 STAR^{e} SYSTEM (Mettler Toledo) under air (50 mL/min) at a heating rate of 10 ºC/min.

Scanning electron microscopy (SEM) images were obtained over gold-coated specimens with FEI INSPECT-F (F50) equipment operating at 5-30 kV, while images of the smallest crystals were taken using transmission electron microscopy (TEM) using FEI Tecnai G^2 F20 operating at 300 kV. The TEM specimens were prepared after repeated dispersion in acetone before being poured onto the holey carbon copper grid.

The porosity was analyzed in a Micromeritics Tristar 3000 instrument with N_2 at -196ºC. The samples were measured after degassing at 200ºC for 8 h under vacuum.

Mercury porosimetry experiments were performed using a Micromeritics Autopore IV 9520. The samples were degassed for 24 h at 100ºC.

The oxygen permeation measurements (cc/m^2·24h·atm) of the films were made by the Technological Institute of Plastics, AIMPLAS. The measurements were performed at 26ºC and 0% RH using the ASTMD3985 standard test method for the O_2 gas permeation rate through plastic film.

The Charpy impact tests were performed using the UNE-EN ISO-179-1 standard with 1eA type test specimens.

3. Results

3.1. Synthesis of JDF-L1

The synthesis of JDF-L1 was first made in the 150 mL autoclave. This synthesis was characterized by SEM (Fig. 2a) and XRD (Fig. 3), confirming that the diffraction pattern corresponded to JDF-L1 and that the sheet size, 5.2 ± 1.2 µm, was slightly higher than that obtained by Rubio et al. (Rubio et al., 2009) in a 35 mL autoclave (approx. sheet size 3 µm). Changing the dimensions of the autoclave subtly modifies the parameters that can influence the nucleation/crystal growth such as the heating rate and homogeneity, the surface/volume relationship of the autoclave or the volume ratio of the gas phase/liquid phase. The thickness of the JDF-L1 sheets obtained also varies slightly with the volume of the autoclave in which the synthesis takes place: 135 ± 25 nm for 35 mL and 175 ± 24 nm for 150 mL. With the 150 mL autoclave, 8 syntheses of JDF-L1 were made obtaining an amount of JDF-L1 of 89 g. The average amount of JDF-L1 obtained in each synthesis was 12.6 ± 0.3 g, giving a yield for Ti of 86.4%. These eight syntheses were analyzed by XRD (not shown) and were similar in all cases with no hint of impurities.

The next stage consisted of performing the synthesis in the 400 mL autoclave. A first synthesis with the same proportions of reagents and seeds was performed as in the synthesis in the 150 mL autoclave. The observations by XRD (Fig. 3) showed that while the X-ray diffractogram corresponded with JDF-L1, this sample contained some impurities (revealed by SEM (not shown)). Therefore, another synthesis was performed doubling the amount of seeds to promote secondary nucleation and to avoid the generation of impurities. SEM showed that this new synthesis had fewer impurities and a sheet size of 5.3 ± 1.7 μm with a thickness of 115 ± 36 nm. The synthesis was repeated 8 times obtaining 378 g of JDF-L1, with an average per synthesis of 47.3 ± 1.8 g and a yield of 93.3% Ti. Therefore, when the volume of the autoclave is higher, the yield is also higher. This is because when working with more material, the amount of solid lost during the filtering and washing stages is proportionally smaller than when working with less material.

3.2. Disaggregation of JDF-L1

In the process of disaggregation at high pH, the sheets charge negatively and the electrostatic repulsion produced favors their disaggregation. However, the reagents employed by Galve et al. (Galve et al., 2011) (CTAB and especially TPAOH) are expensive for disaggregating large amounts of JDF-L1. For this reason, four experiments were performed to check which method was more effective. These experiments are summarized in Table 1.

0.5 g of JDF-L1 was used in all four experiments. The products obtained were analyzed by XRD (Table 1) showing crystalline JDF-L1, except in the case of method 2 where reflections corresponding to CTBA appeared probably due to the need for more intensive washing. SEM observation (Fig. 2b-d) showed that using methods 1, 2 and 3 there

were still significant aggregates of JDF-L1, while employing method 4 most of the JDF-L1 was successfully disaggregated (Fig. 2e).

If disaggregation is effective, the sheets tend to fall horizontally, thereby increasing the intensity of the *00l* type reflections (Fig. 3). Thus, a disaggregation index (I_d) was calculated to compare the disaggregation ability of each method. This is the sum of the *00l* reflection (*001*, *002* and *003*) areas divided by the sum of the previous reflections and the three reflections of greater area of JDF-L1, corresponding to *102*, *201* and *211* reflections.

$$I_d = \frac{A_{001} + A_{002} + A_{003}}{A_{001} + A_{002} + A_{003} + A_{102} + A_{201} + A_{211}}$$

The disaggregation index values were calculated for each method (Table 1), except for method 2 due to the absence of JDF-L1 reflections. The disaggregation index indicated that using method 4 the material was disaggregated to a greater degree, which was consistent with the SEM observations.

Once it was established that the most effective method of disaggregation was that using NaOH (which in turn favored subsequent washing avoiding the use of surfactant CTAB), six processes of disaggregation over 35 g of JDF-L1 in each were carried out. A total of 171 g of disaggregated JDF-L1 with a yield of 81.5% by mass was obtained. The material was disaggregated correctly, presenting sheets with a size of 4.8 ± 0.7 μm. It was observed by SEM that the edges of the sheets had soft shapes, therefore the disaggregated material was examined by TEM to obtain higher resolution (Fig. 2f). These irregularities might be caused by the high pH at which the process is carried out and which may partially dissolve the edges of the crystals.

The BET area of the disaggregated material (16.5 ± 0.1 m^2/g) increased slightly with respect to the BET area of the synthesis (30.1 ± 0.1 m^2/g) although it was similar to the value of 29.6 m^2/g of other synthesized JDF-L1 powders (Rubio et al., 2010). Thus the pore structure was not altered significantly. The ratio of Si/Ti was analyzed by XRF giving values of 2.6 and 2.1 for JDF-L1 and disaggregated JDF-L1, respectively, indicating a slight decrease in the Si value; this was because the disaggregation process with NaOH partially dissolved the silicon in the JDF-L1.

To observe possible changes in the distribution of the interparticle spaces, mercury porosimetry analyses were performed. The specific pore volume in the disaggregated material decreased slightly from 3.6 to 2.7 mL/g (JDF-L1) while the total pore area was constant: 13.6 m^2/g for JDF-L1 and 13.8 m^2/g for disaggregated. Here pores were considered to be the spaces between sheet particles. The decrease in the specific volume of pores in the disaggregated material may be because mercury can penetrate into the gaps between the aggregates of JDF-L1, while in the case of the disaggregated material these gaps do not exist due to the sheet to sheet contact.

Therefore, the method used to disaggregate the JDF-L1 was effective despite a slight partial dissolution of Si. It did not essentially affect the crystal structure of JDF-L1, as verified by XRD, or the porosity of the material, as seen by N_2 adsorption. It was found by mercury porosimetry that the breakdown was effective because the interparticle gaps caused by the aggregates decreased in size.

3.3. Manufacture of films

Firstly Nurel S.A. manufactured pellets of PA6 with a load of 2 wt% of disaggregated JDF-L1. The test pieces for the Charpy impact test were made from these

257 pellets. The JDF-L1@PA6 pellets were observed by SEM (Fig. 4a,b) depicting how the
258 sheets are surrounded by the polyamide, suggesting good interaction. Table 2 shows the
259 results of the Charpy impact test for PA6, JDF-L1@PA6 and PA6 with a typical additive
260 tested by Nurel SA. The name of the additive was not provided for reasons of
261 confidentiality. In the case of using JDF-L1 as an additive, no significant variations were
262 observed in the flexural modulus and bending strength, so that in the manufacture of the
263 films and their subsequent uses there should be no important difference compared to the
264 pure polyamide. The Charpy impact decreased but not enough for the film to be easily
265 broken during use. In the case of the other additive of Nurel SA, flexural modulus and
266 bending strength were increased slightly. This indicated that the resultant polymer is a bit
267 more rigid which is a good property to work with it in the injection; however, this can be a
268 drawback in case of film manufacturing due to the lesser elasticity.

269 Once it was seen that the mechanical properties of PA6 with disaggregated JDF-L1
270 were good enough, films were made. The film made with JDF-L1@PA6 was similar to that
271 of pure PA6. Furthermore, the JDF-L1@PA6 film showed a greater facility for picking up
272 at the end of processing because it exhibited less adherence. Regarding the transparency of
273 the films, the JDF-L1@PA6 showed a slight opacity but allowed good vision through it and
274 reduced light reflection, as shown in Fig. 5. This can be considered as a clear advantage of
275 this composite.

276 Films were analyzed by XRD and SEM to check the dispersion and orientation of
277 the JDF-L1 sheets within the polymer. For the XRD analysis (Fig. 6), 4 samples (4 x 4 cm)
278 of the JDF-L1@PA6 film (21 x 55 cm) were measured. The four samples of film with JDF-
279 L1 had a similar diffraction pattern, so the dispersion of JDF-L1 in the film was correct and

280 there were no areas without its presence. It is also noted that the JDF-L1@PA6 film
281 showed the characteristic reflection of PA6 at 21.8 º and three reflections of JDF-L1
282 corresponding to *00l* type reflections. This indicated a good crystallographic orientation of
283 the JDF-L1 sheets in the polymer which were deposited parallel to each other and
284 perpendicular to the direction of air permeation. This could increase the barrier effect.
285 However, there were evident shifts of 2·theta values in the JDF-L1 reflections which were
286 attributed to deformation in the crystal lattice produced either by the interaction with the
287 polymer or the processing temperature (Castarlenas et al., 2013).There was also a slight
288 change in the 2·theta values of PA6 that could be related to a change in the crystalline
289 phase of PA6 in the presence of fillers (Tung et al., 2005). Similar parallel crystallographic
290 orientations were reported previously in the case of composites of JDF-L1 with polysulfone
291 (Castarlenas et al., 2013) and polyimide (Galve et al., 2011; Galve et al., 2013), a clear
292 advantage of the procedure described here related to the easier and cleaner disaggregation
293 with innocuous NaOH.

294 The XRD results were corroborated by SEM in the JDF-L1@PA6 film (Fig. 4c,d).
295 There was a good dispersion of the JDF-L1 sheets throughout the film thickness (52 μm)
296 and a good orientation since they were positioned in the polymer matrix perpendicular to
297 the gas flow, increasing the potential barrier effect. In Fig. 4d, a JDF-L1 sheet is
298 surrounded by PA6 and no gap can be appreciated at the JDF-L1-polymer interface.

299 The barrier effect of these films was studied by O_2 permeation through the film. The
300 film having the lowest permeation of O_2 will be the most suitable for use in food packaging
301 and the food will keep longer in its original condition. The O_2 permeation results (6
302 measurements) for the PA6 and JDF-L1@PA6 films were 28.4 ± 2.4 and 28.5 ± 1.6

cc/m^2·24h·atm, respectively. The permeability results (estimated by 1 Barrer = 10^{-11}·(cm^3 O_2 STP)·cm·cm^{-2}·s^{-1}·mmHg^{-1} with film thickness 52 μm) for the PA6 and JDF-L1@PA6 films were 0.022 ± 0.002 and 0.022 ± 0.001 Barrer. Both films showed similar values of permeation and permeability so that the addition of disaggregated JDF-L1 in these conditions did not lead to an improvement in the barrier effect of the film. This may be because the JDF-L1 barrier effect was counteracted by nanometer gaps created at the JDF-L1-polymer interface. This was not the case when working with copolyimide (Galve et al., 2011), which may be because this polymer interacts better with JDF-L1 or because it had a higher permeability than polyamide. Thus the JDF-L1 showed a barrier effect since the permeation through possible nanometric gaps would have been similar or even lower than permeability of the polymer. In the previous copolyimide study, the pure polymer membrane had a permeation of O_2 at 35 °C of 91 Barrer decreasing to 38 Barrer in the case of the JDF-L1-copolyimide (5% by mass) membrane.

4. Conclusions

A JDF-L1 synthesis procedure has been developed in which about 50 g are obtained in a single synthesis of 24 h. A procedure has also been developed for disaggregating the aggregates of JDF-L1 using a cheap and common reagent such as NaOH. With the disaggregated JDF-L1 sheets, 2 wt% JDF-L1@PA6 composites were prepared. Pure PA6 and JDF-L1@PA6 were analyzed mechanically and no significant variations were observed in the flexural modulus and bending strength. This means that in the manufacture of films and their subsequent uses there should be no difference between using the composite material or the pure polyamide. The composite films were manufactured and analyzed by XRD and SEM to check the dispersion and crystallographic orientation of the JDF-L1

sheets. The four samples of film with JDF-L1 had a similar diffraction pattern with a good dispersion and orientation of JDF-L1 sheets in the film. Pure PA6 and JDF-L1@PA6 films had a similar O_2 permeation value, so that the addition of disaggregated JDF-L1 in these conditions did not improve the barrier effect of the film. However, unlike the case with other additives, it did not worsen the mechanical and transparency properties of the film.

Given the good dispersion and orientation of the sheets of the JDF-L1@PA6 composite, these types of films could in future be applied to packaging due to their similar mechanical properties and barrier effect as those of polyamide 6. They also provide other properties such as a biocide effect (Pérez-Carvajal et al., 2012) and, if used in combination with other fillers, a synergy effect improving the dispersion of the filler (Galve et al., 2013).

5. Acknowledgments

Financial support from the Spanish Ministry of Economy and Competitiveness (TRA2009_0049, MAT2013-40556-R), the European Social Fund (ESF) through the Aragón Government (GA-LC-019/2011 and DGA, T05) and Obra Social la Caixa, is gratefully acknowledged. The authors would like to thank the University of Zaragoza for the use of the Servicio General de Apoyo a la Investigación-SAI and the Laboratorio de Microscopías Avanzadas (LMA) at the INA.

6. References

Aldousiri, B., Dhakal, H.N., Onuh, S., Zhang, Z.Y., Bennett, N., Richardson, M.O.W., 2012. Effect of layered silicate reinforcement on the structure and mechanical properties of spent polyamide-12 nanocomposites. Composites Part B: Engineering 43, 1363-1367.

347 Alix, S., Follain, N., Tenn, N., Alexandre, B., Bourbigot, S., Soulestin, J., Marais, S., 2012. Effect
348 of Highly Exfoliated and Oriented Organoclays on the Barrier Properties of Polyamide 6
349 Based Nanocomposites. The Journal of Physical Chemistry C 116, 4937-4947.
350 Anderson, M.W., Terasaki, O., Ohsuna, T., Malley, P.J.O., Philippou, A., Mackay, S.P., Ferreira,
351 A., Rocha, J., Lidin, S., 1995. Microporous titanosilicate ETS-10: A structural survey.
352 Philosophical Magazine Part B 71, 813-841.
353 Cai, G., Dasari, A., Yu, Z.-Z., Du, X., Dai, S., Mai, Y.-W., Wang, J., 2010. Fire response of
354 polyamide 6 with layered and fibrillar nanofillers. Polymer Degradation and Stability 95,
355 845-851.
356 Castarlenas, S., Gorgojo, P., Casado-Coterillo, C., Masheshwari, S., Tsapatsis, M., Tellez, C.,
357 Coronas, J., 2013. Melt Compounding of Swollen Titanosilicate JDF-L1 with Polysulfone
358 To Obtain Mixed Matrix Membranes for H-2/CH4 Separation. Ind. Eng. Chem. Res. 52,
359 1901-1907.
360 Centi, G., Perathoner, S., 2008. Catalysis by layered materials: A review. Microporous and
361 Mesoporous Materials 107, 3-15.
362 Corma, A., Fornes, V., Martinez-Triguero, J., Pergher, S.B., 1999. Delaminated zeolites:
363 Combining the benefits of zeolites and mesoporous materials for catalytic uses. J. Catal.
364 186, 57-63.
365 Corma, A., Fornes, V., Jorda, J.L., Rey, F., Fernandez-Lafuente, R., Guisan, J.M., Mateo, C., 2001.
366 Electrostatic and covalent immobilisation of enzymes on ITQ-6 delaminated zeolitic
367 materials. Chem. Commun., 419-420.
368 Choi, S., Coronas, J., Jordan, E., Oh, W., Nair, S., Onorato, F., Shantz, D.F., Tsapatsis, M., 2008.
369 Layered silicates by swelling of AMH-3 and nanocomposite membranes. Angew. Chem.-
370 Int. Edit. 47, 552-555.

371 Choudalakis, G., Gotsis, A.D., 2009. Permeability of polymer/clay nanocomposites: A review.
372 European Polymer Journal 45, 967-984.
373 Daud, W., Bersee, H.E.N., Picken, S.J., Beukers, A., 2009. Layered silicates nanocomposite matrix
374 for improved fiber reinforced composites properties. Compos. Sci. Technol. 69, 2285-2292.
375 Echegoyen, Y., Nerín, C., 2013. Nanoparticle release from nano-silver antimicrobial food
376 containers. Food and Chemical Toxicology 62, 16-22.
377 Ferdov, S., Kostov-Kytin, V., Petrov, O., 2002. A rapid method of synthesizing the layered
378 titanosilicate JDF-L1. Chem. Commun., 1786-1787.
379 Galve, A., Sieffert, D., Vispe, E., Tellez, C., Coronas, J., Staudt, C., 2011. Copolyimide mixed
380 matrix membranes with oriented microporous titanosilicate JDF-L1 sheet particles. J.
381 Membr. Sci. 370, 131-140.
382 Galve, A., Sieffert, D., Staudt, C., Ferrando, M., Guell, C., Tellez, C., Coronas, J., 2013.
383 Combination of ordered mesoporous silica MCM-41 and layered titanosilicate JDF-L1
384 fillers for 6FDA-based copolyimide mixed matrix membranes. J. Membr. Sci. 431, 163-
385 170.
386 Giannelis, E.P., 1996. Polymer layered silicate nanocomposites. Adv. Mater. 8, 29-35.
387 Jeong, H.K., Krych, W., Ramanan, H., Nair, S., Marand, E., Tsapatsis, M., 2004. Fabrication of
388 polymer/selective-flake nanocomposite membranes and their use in gas separation. Chem.
389 Mat. 16, 3838-3845.
390 Kojima, Y., Usuki, A., Kawasumi, M., Okada, A., Fukushima, Y., Kurauchi, T., Kamigaito, O.,
391 1993. Mechanical-properties of nylon 6-clay hybrid. J. Mater. Res. 8, 1185-1189.
392 LeBaron, P.C., Wang, Z., Pinnavaia, T.J., 1999. Polymer-layered silicate nanocomposites: an
393 overview. Applied Clay Science 15, 11-29.

394 Lin, Z., Rocha, J., Brandao, P., Ferreira, A., Esculcas, A.P., deJesus, J.D.P., Philippou, A.,
395 Anderson, M.W., 1997. Synthesis and structural characterization of microporous umbite,
396 penkvilksite, and other titanosilicates. J. Phys. Chem. B 101, 7114-7120.
397 Mihindukulasuriya, S.D.F., Lim, L.T., 2014. Nanotechnology development in food packaging: A
398 review. Trends in Food Science & Technology 40, 149-167.
399 Park, K.-W., Jung, J., 2011. Preparation of transparent PVC-titanosilicate nanocomposites by
400 interlamellar silylation of layered titanosilicate. J Inorg Organomet Polym 22, 119-124.
401 Pérez-Carvajal, J., Lalueza, P., Casado, C., Téllez, C., Coronas, J., 2012. Layered titanosilicates
402 JDF-L1 and AM-4 for biocide applications. Applied Clay Science 56, 30-35.
403 Roberts, M.A., Sankar, G., Thomas, J.M., Jones, R.H., Du, H., Chen, J., Pang, W., Xu, R., 1996.
404 Synthesis and structure of a layered titanosilicate catalyst with five-coordinate titanium.
405 Nature 381, 401-404.
406 Rocha, J., Lin, Z., 2005. Micro- mixed octahedral-pentahedral-tetrahedral framework silicates. Rev.
407 Mineral Geochem. 57, 173-201.
408 Roth, W.J., Nachtigall, P., Morris, R.E., Čejka, J., 2014. Two-Dimensional Zeolites: Current Status
409 and Perspectives. Chem. Rev. 114, 4807-4837.
410 Rubio, C., Casado, C., Uriel, S., Tellez, C., Coronas, J., 2009. Seeded synthesis of layered
411 titanosilicate JDF-L1. Materials Letters 63, 113-115.
412 Rubio, C., Casado, C., Gorgojo, P., Etayo, F., Uriel, S., Tellez, C., Coronas, J., 2010. Exfoliated
413 Titanosilicate Material UZAR-S1 Obtained from JDF-L1. European Journal of Inorganic
414 Chemistry 2010, 159-163.
415 Rubio, C., Zornoza, B., Gorgojo, P., Téllez, C., Coronas, J., 2015. Separation of H_2 and CO_2,
416 Containing Mixtures with Mixed Matrix Membranes Based on Layered Materials Current
417 Organic Chemistry 18, 2351-2363.

418 Tung, J., Gupta, R.K., Simon, G.P., Edward, G.H., Bhattacharya, S.N., 2005. Rheological and
419 mechanical comparative study of in situ polymerized and melt-blended nylon 6
420 nanocomposites. Polymer 46, 10405-10418.
421 Usuki, A., Kojima, Y., Kawasumi, M., Okada, A., Fukushima, Y., Kurauchi, T., Kamigaito, O.,
422 1993. Synthesis of Nylon 6-clay hybrid. J. Mater. Res. 8, 1179-1184.
423 Vähä-Nissi, M., Pitkänen, M., Salo, E., Kenttä, E., Tanskanen, A., Sajavaara, T., Putkonen, M.,
424 Sievänen, J., Sneck, A., Rättö, M., Karppinen, M., Harlin, A., 2014. Antibacterial and
425 barrier properties of oriented polymer films with ZnO thin films applied with atomic layer
426 deposition at low temperatures. Thin Solid Films 562, 331-337.
427 Veltri, M., Vuono, D., De Luca, P., Nagy, J.B., Nastro, A., 2006. Typical data of a new
428 microporous material obtained from gels with titanium and silicon. J. Therm. Anal.
429 Calorim. 84, 247-252.
430 Wang, Z., Pinnavaia, T.J., 1998. Hybrid organic-inorganic nanocomposites: Exfoliation of
431 magadiite nanolayers in an elastomeric epoxy polymer. Chem. Mat. 10, 1820-1826.
432 Wu, P., Nuntasri, D., Ruan, J.F., Liu, Y.M., He, M.Y., Fan, W.B., Terasaki, O., Tatsumi, T., 2004.
433 Delamination of Ti-MWW and high efficiency in epoxidation of alkenes with various
434 molecular sizes. J. Phys. Chem. B 108, 19126-19131.
435 Zhang, H., Yang, L., 2012. Immobilization of nanoparticle titanium dioxide membrane on
436 polyamide fabric by low temperature hydrothermal method. Thin Solid Films 520, 5922-
437 5927.

438

439

FIGURE CAPTIONS

Figure 1. JDF-L1 framework structure simulated with PowderCell 2.4 software using structural information (Roberts et al., 1996). (Red: O; Green: Ti; Yellow: Si; Blue: Na)

Figure 2. SEM images of: a) Synthesized JDF-L1 in the autoclave of 150 mL. Disaggregated JDF-L1: b) CTAB + TPAOH; c) CTAB + NaOH; d) TPAOH and e) NaOH. f) TEM of disaggregated JDF-L1

Figure 3. XRD of simulated JDF-L1 (PowderCell 2.4 software using structural information (Roberts et al., 1996)), synthesized JDF-L1 with different autoclave volume and disaggregated JDF-L1

Figure 4. SEM images of: a, b) Pellets of JDF-L1@PA6. c, d) JDF-L1@PA6 film

Figure 5. Image of both films: left, pure PA6 and right JDF-L1@PA6

Figure 6. XRD of disaggregated JDF-L1, PA6 film and samples of JDF-L1@PA6 film

TABLES

Table 1. Methods to disaggregate the JDF-L1 used and disaggregation index

	Disaggregation agent	**Solution volume/JDF-L1 mass (mL/g)**	**XRD**	**SEM appearance**	**Disaggregation index**
JDF-L1					0.35
Method 1	CTAB + TPAOH	30.0	✓	X	0.52
Method 2	CTAB + NaOH	18.6	X	X	
Method 3	TPAOH	24.0	✓	X	0.58
Method 4	NaOH	12.7	✓	✓	0.68

Table 2. Charpy impact test results for PA6, JDF-L1@PA6 and additive@PA6 samples

Sample	Flexural modulus (MPa)	Bending strength (MPa)	Charpy impact CE 23ºC (kJ/m^2)
PA6	2902	113	4.0
JDF-L1@PA6	2731	106	3.3
additive@PA6	2936	114	4.2

FIGURES

FIGURE 1

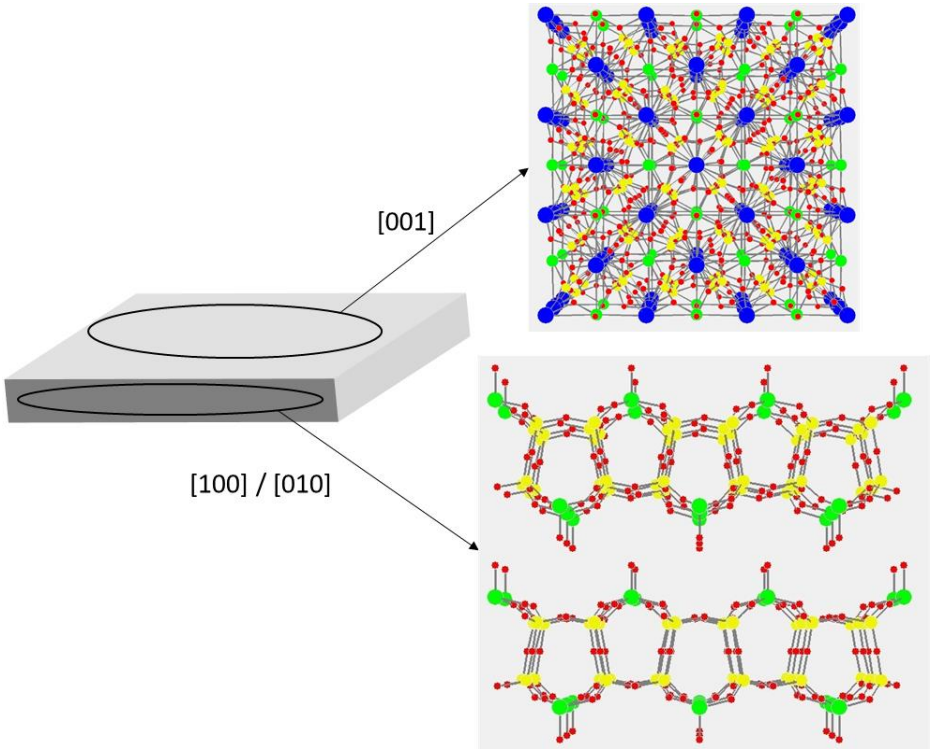

FIGURE 2

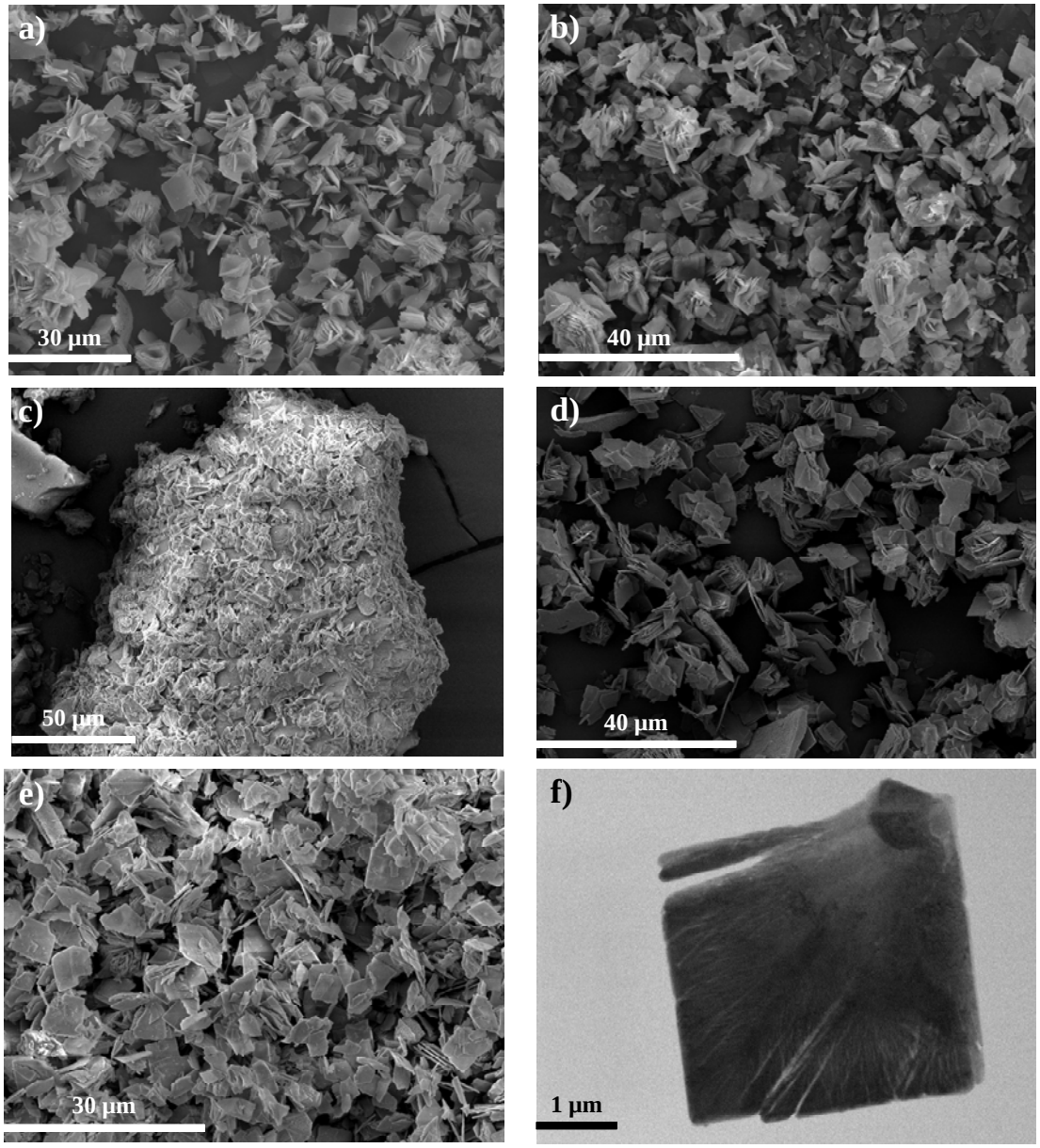

FIGURE 3

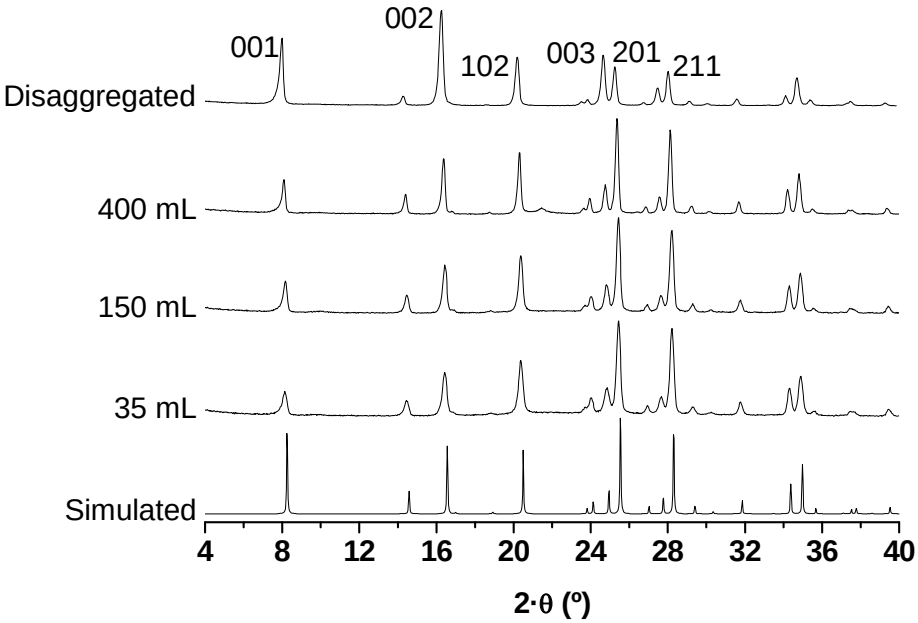
001
002
102
003
201
211
Disaggregated
400 mL
150 mL
35 mL
Simulated
4
8
12
16
20
24
28
32
36
40
2·θ (º)

FIGURE 4

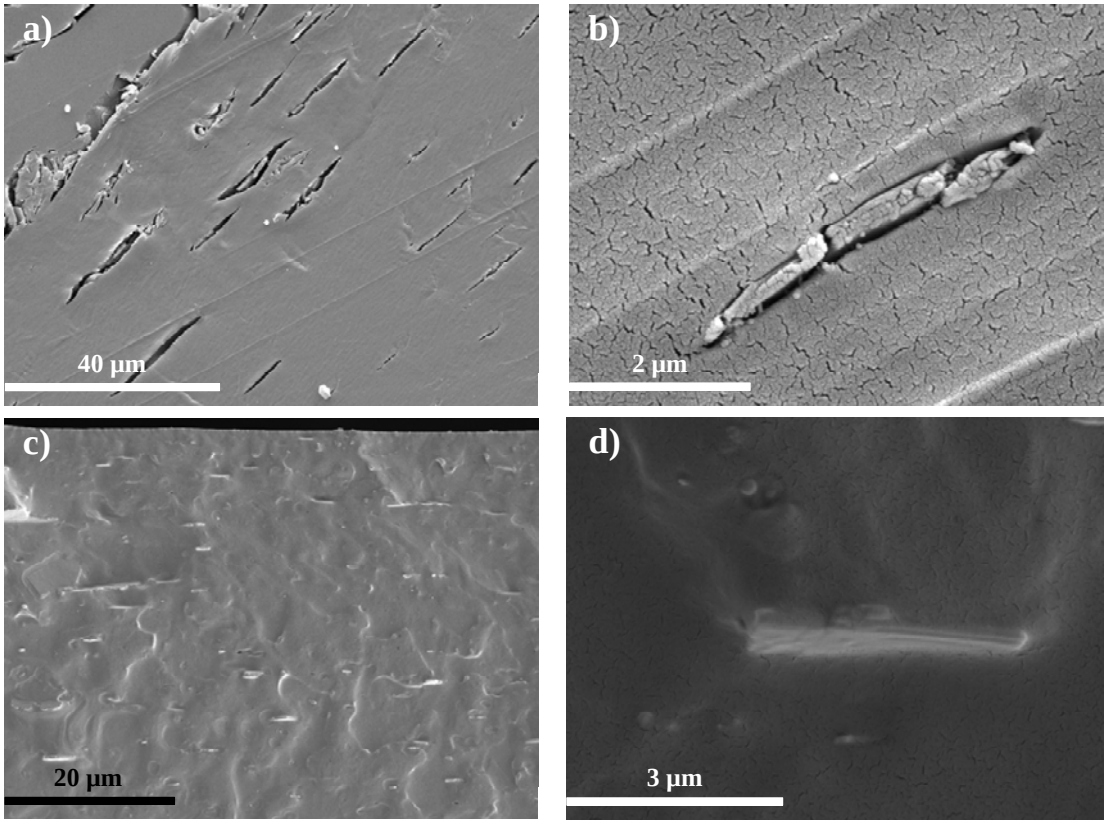

FIGURE 5

FIGURE 6

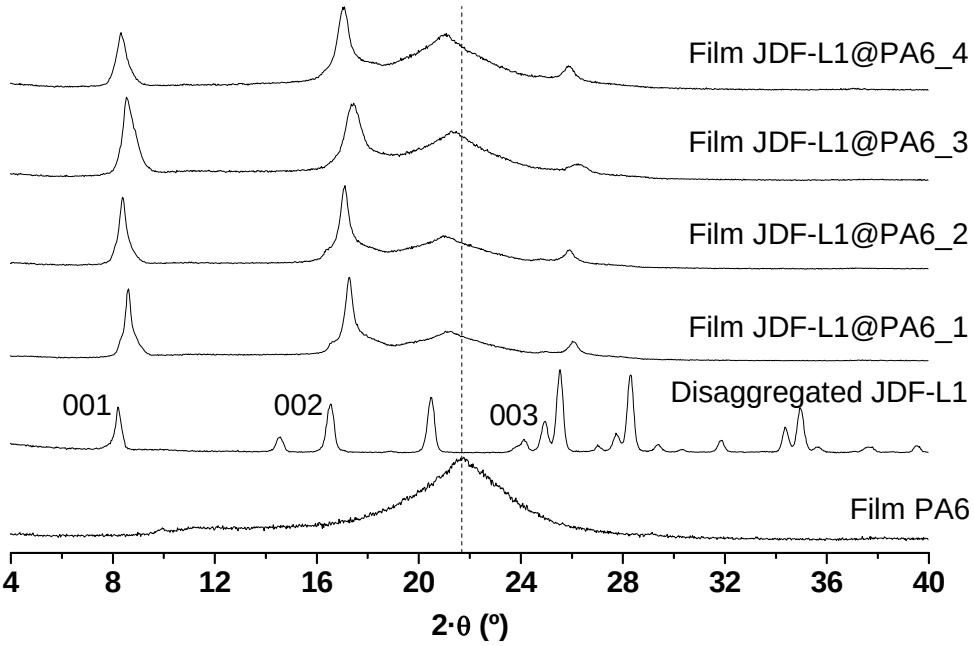
Film JDF-L1@PA6_4
Film JDF-L1@PA6_3
Film JDF-L1@PA6_2
Film JDF-L1@PA6_1
Disaggregated JDF-L1
Film PA6
001
002
003
4
8
12
16
20
24
28
32
36
40
2·θ (º)

Graphical abstract